

Fast LLM Post-training via Decoupled and Fastest-of-N Speculation

Rongxin Cheng^{1,2}, Kai Zhou², Xingda Wei^{*1}, Siyuan Liu¹, Mingcong Han^{1,2}, Mingjing Ai³, Yeju Zhou², Baoquan Zhong², Wencong Xiao², Rong Chen¹, and Haibo Chen¹

¹Institute of Parallel and Distributed Systems, Shanghai Jiao Tong University

²ByteDance Seed

³Unaffiliated

Abstract

Rollout dominates the training time in large language model (LLM) post-training, where the trained model is used to generate tokens given a batch of prompts. This work, SPECACTOR, achieves fast rollout with speculative decoding that deploys a fast draft path to accelerate the unparallelizable generation, while the correctness is guaranteed by fast parallel verification of the outputs with the original model. SPECACTOR addresses two foundational challenges that hinder speculation efficiency: (1) a *Decoupled speculation* method that overcomes the computation inefficiency issue when executing speculative decoding with relative large per-worker batch size—a common configuration in training but unfriendly to speculation, and (2) a *Fastest-of-N speculation* method that selects and combines different draft methods according to the rollout progress to approximate the optimal draft method even when the best one is unknown a priori. Extensive evaluations on production traces show that SPECACTOR accelerates mean rollout speed by 2.0–2.4 \times , with up to 2.7 \times speedup, over common post-training baselines. The results are consistent across both dense and MoE models and across different RL algorithms. Notably, SPECACTOR is 1.1–2.6 \times faster compared to vanilla speculative rollout in different traces. The accelerated rollout achieves 1.4–2.3 \times faster end-to-end training time.

1 Introduction

Large foundational models like LLMs have demonstrated remarkable accuracy across a wide range of tasks including writing [46], coding [51], and many others [45, 63, 33, 24]. Post-training these models with reinforcement learning (RL) has become a key pillar in the training pipeline to further enhance model capabilities in challenging reasoning tasks [15].

Rollout is a key and performance-dominant phase in post-training (§2.2): at each step, the system feeds the model with a batch of prompts representing target problems (e.g., math or coding problems) to be solved. The model then generates tokens for each prompt in an attempt to solve them. When rollout finishes, the generated tokens are evaluated and the

model is updated accordingly. Rollout naturally parallelizes the batch across multiple workers.

Problem statement and current solutions (§2.2). Rollout accounts for 75–80% of the post-training time. This lengthy and inefficient execution is primarily due to long tails in generation and is further exacerbated by idle GPU time, caused by waiting for the slowest worker to finish. The long tail stems from difficulty variation, with some problems requiring more tokens than others to solve. Therefore, one worker may finish its assigned prompts quickly, while another takes much longer to complete. Importantly, waiting for all requests before updating the model is necessary to ensure rapid and stable training convergence [52, 54, 71].

Given this hard constraint, we ask a specific but important question: *how to accelerate rollout in LLM post-training without changing how the model is trained?*

Existing *algorithm-agnostic* solutions fall into two categories, neither of which adequately addresses the issue given the recent trend of ever-growing generation length as LLMs are trained to solve more complex problems [28, 41, 13]. The first category is *overlapping*, which utilizes idle GPUs in the rollout for other phases in the training pipeline [80]. It has been proven effective in short-context RL training but less effective in long-tailed training because it does not accelerate rollout directly, yielding 1.1 \times average speedup. The second category leverages *parallelism*, i.e., utilizing idle or over-provisioned GPUs to accelerate post-training [6]. Unfortunately, the speedup is still limited (e.g., up to 1.2 \times with doubled GPUs) because LLM generation is memory-bound and thus cannot fully utilize the extra computation power.

This work: lossless and efficient speculative rollout. We present SPECACTOR, a fast rollout system that retrofits speculative decoding [7, 8, 70, 47]—a common technique for accelerating LLM inference—to LLM post-training. Specifically, speculative decoding employs a fast path for sequential generation (decoding): First, a “draft” model much smaller than the trained one generates a sequence of n draft tokens. Then, the trained model verifies these tokens. Once accepted, these tokens are treated as generated by the trained model. The rationale is that verifying n tokens is typically faster than generating them—although using the same model—because

^{*}Xingda Wei is the corresponding author (wxdwfc@sjtu.edu.cn).

verification processes multiple tokens in parallel.

It is important to note that speculative decoding can provide lossless generation as the original decoding via exact token matching [65]. Moreover, the drafters are available at post-training [31, 43]: pre-training pipeline generates both small and large models, following established scaling practices [61, 67]. Besides, n-gram-based drafters are model-free [2, 25].

While intuitive and effective in inference, applying vanilla speculative decoding to rollout yields only 10 % speedup at worst on common production configurations (§5.2) due to the following challenges. We further address them with two contributions.

Computation-efficient rollout via decoupled speculation (§4.1). First, the effectiveness of speculative decoding depends mainly on the verification overhead, which is proportional to the per-worker batch size. However, on common training configurations, e.g., per-worker batch size 128, (see Figure 5 (a)), the verification could become slower than generation due to reaching the GPU computation limit, also noticed by recent works [36, 40]. Although the batch size gradually decreases during rollout as prompts finish, it remains relatively large (e.g., ≥ 64) for a considerable portion of the rollout time (e.g., 20 %), so we need efficient execution on batch configurations that are unfriendly to speculation.

Our key observation is that there exist opportunities to accelerate verification because vanilla speculative execution limits the GPU time provisioned to (compute-hungry) verification due to a coupled draft-*n*-then-verify dependency: the verifier must wait for GPU-underutilized drafter jobs. Such a dependency is necessary to ensure high speculation efficiency for *all requests* (required in inference [40]) because without it, the drafter could further waste all $[n, \dots]$ tokens if verification rejects one token in $[1, n]$. However, such a dependency is overly conservative for rollout where only the batch completion time matters, so trading off a few requests to accelerate others is beneficial. Based on this, we propose decoupled speculation to relax the dependency between draft and verification. The drafter can continue drafting without waiting for verification to finish, thereby allowing subsequent verifications to start earlier to maximize GPU time provisioned to verification. The decoupling comes at the cost of decreased acceptance rate due to more in-flight unverified tokens. Fortunately, many requests only have a slightly decreased acceptance rate, so the computation gain offsets the acceptance loss. Moreover, we further propose a feedback-based draft window mechanism to dynamically minimize wasted tokens due to such aggressive drafting via online reconfiguration.

Effective draft adaptation via Fastest-of-N speculation (§4.2). Second, speculative decoding has multiple candidate draft methods, and it is a common practice to select a single drafting method for all requests based on profiling or experience [31, 43]. However, we found in rollout that differ-

ent requests suit different draft methods, so using one fixed method might lead to inefficient speculation for stragglers. However, it is challenging to select the optimal one for all requests because for each request, the optimal method not only depends on how fast the drafter is, but also on the acceptance rate of verification. The latter is unknown in advance as it depends on the model output. Meanwhile, it is impractical to run multiple draft methods for each request as it requires proportional extra verifiers and thus extra GPUs.

We propose Fastest-of-N speculation that approximates the best draft methods for all requests with the following three techniques. First, we propose a new abstraction called *draft ladder* that establishes a mapping from various acceptance rates to speedup given a pool of draft methods, which can be constructed offline. Given the ladder, at the beginning of rollout, we select one estimated fastest draft method using the average acceptance rate of all requests profiled so far. The rationale is that even though each requests' acceptance rate varies significantly, the average acceptance rate over a (large) batch of requests is statistically stable [22]. Thus, the selected draft method is likely to be close to the optimal for the batch. Finally, when the batch size decreases during rollout and the initial selection becomes suboptimal, we utilize the freed GPUs from finished workers to launch more draft methods in parallel for long-tailed requests, and the request finishes when the fastest draft method generates the end token (EOS) that is accepted by the verifier. Running multiple draft methods in parallel increases the likelihood of selecting the fastest method with unknown acceptance rates, while utilizing the idle GPUs avoids extra GPU usage.

Demonstration. SPECACTOR preserves the exact rollout process for any training algorithm, so algorithm designers can seamlessly use it without worrying about potential accuracy loss. We built SPECACTOR on veRL [55], a state-of-the-art post-training framework. SPECACTOR is easy to integrate into other training frameworks, as it serves as a drop-in replacement for the inference component of any post-training pipeline, without requiring changes to the training logic. Extensive evaluations show that on various real-world training traces and common post-training algorithms including GRPO [54, 13], DAPO [71], and PPO [52], compared to the state-of-the-art solutions like veRL and RLHFuse, SPECACTOR accelerates the end-to-end training time by 1.4–2.3 \times . Also, we are up to 2.6 \times faster than vanilla speculative rollout baselines in different traces.

2 Background and Motivation

2.1 LLM post-training

Generation with LLM. Large Language Models (LLMs) generate responses (termed *tokens*) through *prefill* and *decode* phases. The prefill phase processes the initial input (termed *prompt*) to generate the first token. The decode phase then iteratively generates subsequent tokens in an auto-regressive

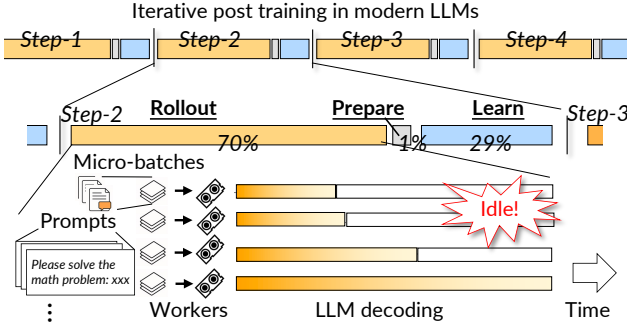


Figure 1: An illustration of the rollout process in LLM post-training.

fashion by combining previous output tokens with the original input as the new input. The decode phase terminates upon generating an end-of-sequence token.

Post-training workflow. Leading LLMs are post-trained with reinforcement learning (RL) with multiple steps of execution, where each step follows an identical three phases [15, 42, 81, 55]:

1. Rollout. The process treats the trained model as actor and generates tokens from a sampled batch of pre-defined prompts using LLM decoding. The tokens are used to solve specific tasks like math problems. To accelerate rollout, the sampled batch is divided into smaller micro-batches (*batch*¹) and processed concurrently by multiple rollout workers. Each worker deploys the model on one or more GPUs using model parallelism if necessary [55].

Two aspects regarding rollout batch need to be noted. First, to improve efficiency, production RL training applies a relatively large rollout batch size per step to find sufficient positive rewards [30, 54, 69, 71, 78], e.g., a typical 32B task sets the per-step total batch size to 8 K [71, 72]. Second, each prompt is typically seen only once or twice (i.e., common training involves just 1–2 epochs [13]), limiting the effectiveness of n-gram-based methods like experience replay [37, 21].

2. Prepare. In the prepare phase, the rollout results are fed into a set of judges [54, 71, 73, 76] (e.g., a separate reward model) to generate rewards [52, 5], which are the arithmetic signals that guide the parameter optimization. These judges are lightweight; for example, the reward models only compute a forward pass, rather than auto-regressive generation, so the time required is negligible in a training step.

3. Learn. Given the signals from the prepare phase, the learning phase calculates the loss and updates the LLM parameters with a backward pass. The updated parameters are then used in the next rollout step.

2.2 Analysis of post-training and current solutions

Rollout dominates execution time in post-training and suffers significant GPU wastes. Figure 2 (a) analyzes

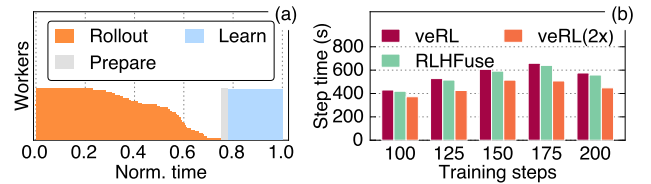


Figure 2: (a) The long rollout in post-training and (b) the training latency of various steps in DAPO-32B-20K training trace (detailed setups described in §5.1).

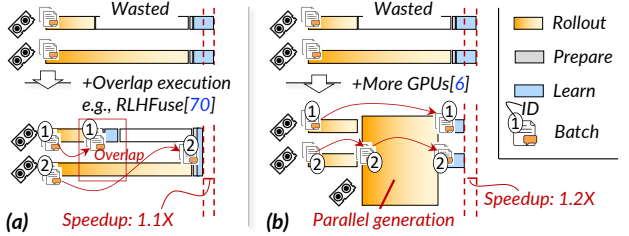


Figure 3: (a) An illustration of accelerating post-training via overlapped execution and (b) an illustration of accelerating rollout through scaling to more GPUs.

the contribution of total post-training time in typical training tasks: rollout contributes 70–80 % of the total training time. Since post-training could last for days on hundreds of thousands of GPUs, accelerating rollout is critical to reducing the overall training cost.

There exists significant space for improvement for rollout because many GPUs are idle during the rollout phase due to the long-generation tail problem. Figure 2 (a) shows the GPU bubble in long-tailed rollout: on a DAPO-32B-20K trace, we observed averagely 50 % of the total GPU time is wasted on waiting for the slowest worker to finish. Rollout time differs significantly across workers even with the same per-worker batch size, because the number of tokens required to solve different tasks varies significantly, and the exact number is hard to predict in advance as they are determined by the LLM outputs. Moreover, the waste increases as training progresses because as the model becomes "smarter", it tends to generate more tokens to solve particular tasks [13].

Reducing GPU waste via overlapping achieves a minor speedup for long-tail generation. An intuitive solution to reduce wasted GPU time is to overlap other phases with the current rollout: As shown in Figure 3 (a), representative solutions like RLHFuse [80] utilize the idle workers to execute the prepare and learn phases of finished batches (e.g., batch ①), overlapping these phases from fast workers with the rollout of slower workers. While such an overlap cannot accelerate the rollout phase, which is bottlenecked by the slowest worker, it reduces the end-to-end training time because once the slowest rollout finishes, more GPUs can participate in accelerating the remaining phases of the slowest batch (e.g., batch ②).

However, the speedup from overlapping is limited because the accelerated prepare and learn phases only contribute a small portion of the overall training time (e.g., about 5% in Figure 2 (a)). As a result, RLHFuse only accelerates post-

¹Since we only refer to micro-batches in the following content, we use the more general term *batch* to indicate micro-batch without loss of generality.

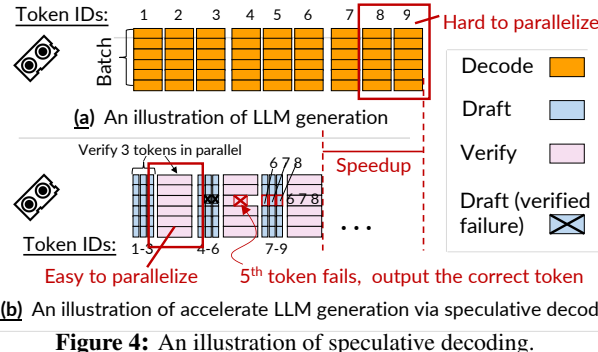


Figure 4: An illustration of speculative decoding.

training by 3 % in traces with long response budget, with GPU time still wasted, as shown in Figure 2 (b).

The sequential-generation nature of rollout is the key obstacle for acceleration. Another intuitive solution is to dynamically add more computation resources to accelerate the long-tailed workers: as shown in Figure 3 (b), once a rollout worker finishes its assigned batch (e.g., batch ①), it can help accelerate the generation of unfinished batches (e.g., batch ②) using parallel LLM generation techniques like sequence parallelism [64]. Moreover, current works [6] aggressively add more GPUs (e.g., by allocating spot instances) to accelerate the slow rollout workers without waiting for more GPUs to become idle. In our example, three workers now process the rollout of batch ②. Unfortunately, as shown in Figure 2 (b), even if we provision $2 \times$ GPUs for rollout, the end-to-end training time is only improved by 1.2–1.3 \times . The limited speedup is rooted in the sequential, memory-bound nature of rollout: tokens must be generated one-by-one, leaving little room for tensor or sequence parallelism [64] due to the extra communication overhead. Moreover, data and pipeline parallelism can hardly accelerate when memory-bound.

Current systems either suffer from limited speedup or adopt lossy acceleration methods like off-policy training or truncating tailed generations, as summarized in §6. We seek an algorithm-agnostic system solution for fast rollout.

3 Design Rationale and System Overview

Opportunity: speculative decoding for rollout [9, 32, 36, 40, 57, 44]. It is a common technique to accelerate sequential LLM generation: As detailed in Figure 4 (a), the original generation iteratively generates tokens for the current batch using the model being trained. With speculative decoding (b), we first generate a sequence of tokens using a fast draft method, e.g., with a smaller model, as detailed in §4.1. The drafted tokens are then verified by the trained model before being accepted as the generated tokens.

Since the verification can be performed on multiple tokens in parallel, its time is similar to or less than that of generating a single token if GPU computation is not the bottleneck. Thus,

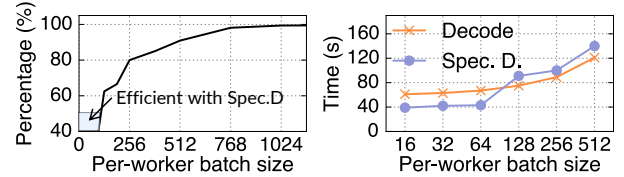


Figure 5: (a) Distribution of the initial per-worker batch sizes of post-training traces in the last 6 months in a large production cluster. (b) The acceleration of speculative rollout given such a batch size on a Qwen2.5-32B checkpoint.

if tokens are accepted, speculative decoding is much faster than the original generation, as shown in the right half of Figure 6 (b). On the other hand, if the verification rejects the drafted tokens, e.g., the 5th token for request 3 in our example, the rejected token and draft tokens after it, e.g., tokens 5–6, will be discarded, and the drafter starts from token 6—as the verification will provide a correct 5th token.

Challenge #1: Limited speedup for typical training configurations. While intuitive, we found adopting state-of-the-art speculative decoding techniques [2, 16, 34, 43] in rollout results in limited speedup, because the speculation verification is inefficient on per-worker batch sizes common in training (see Figure 6 (a)). Figure 5 (a) shows the distribution of per-worker batch sizes collected from production post-training jobs, and (b) compares the time of generation at most 4,096 tokens using speculative decoding and the original generation on a Qwen2.5-32B model. We can see that for common per-worker batch sizes (e.g., 128), speculative decoding brings no or negative gain. The reason is that the verification time increases more significantly with the increased request batch size than others, as shown in Figure 6 (d), because verification introduces a larger token batch than original generation.

One may notice that the per-worker batch size decreases during rollout as more requests finish. However, in at least 20% of the rollout time, the batch size is relatively large in our DAPO-32B-20K trace (see §5.1), which still calls for efficient speculative decoding acceleration. In training, even a tiny acceleration matters due to the potential of saving many GPU hours.

Our solution: decoupled speculation (§4.1). As we have mentioned in the introduction, we decouple the dependency between drafting and verification, which allows us to fully utilize GPUs for speculative decoding. As shown in Figure 6 (c), unlike traditional coupled execution where the drafter must wait for the verifier, we (1) distribute the drafter and verifier to separate GPUs and (2) allow the drafter to aggressively continue without waiting for the verifier. Such an execution scheme provides more GPU time to the verifier because we only need to allocate a few GPUs for the drafter to avoid many GPU executions being GPU-underutilized during drafting. Note that for the same set of GPUs, decoupled execution

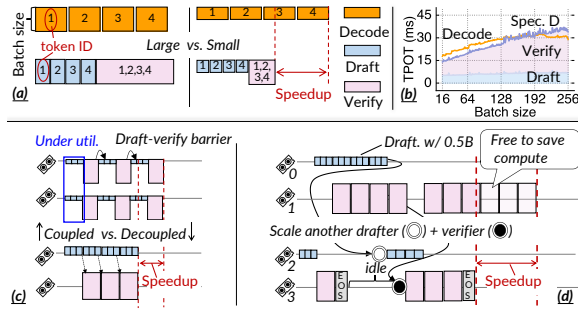


Figure 6: (a) An illustration of the limited speedup of speculative decoding with increased verification costs due to increased batch size. (b) A TPOT (Time Per Output Token) analysis of speculative and normal decoding of Qwen2.5-32B with different batch sizes. (c) An illustration of how decoupled execution reduces GPU underutilization due to the drafter. (d) An illustration of how Fastest-of-N speculation works with finished batches.

increases the per-worker batch size for the verifier: in our example, the batch size is doubled. This does not offset the gain brought by decoupling because verification with a 2 \times batch (from 128 to 256) only incurs a 1.4 \times higher latency (as shown in Figure 6 (b)). Besides, our placement method further minimizes the cost by configuring an appropriate parallelism that distributes the verification across more GPUs.

Decoupled speculative decoding faces the challenge of wasting more GPU resources upon possible decreased acceptance rates. In the example in Figure 6 (c), if a token in positions 1–3 is mis-specified, extra drafted tokens (4–6) will be discarded, which could not happen in a coupled speculation. Fortunately, we found it has little impact on many requests since their acceptance rates remain high, so the speedup of decoupled execution offsets the loss due to waste, still enabling a rapid reduction in the per-worker batch size. To further cope with requests that suffer from significantly decreased acceptance rates, we only relax but not fully discard the draft-verify dependency, using a draft window to control the aggressive generation, i.e., the drafter is only allowed to be ahead of the verifier by a certain number of tokens. Our per-request reconfiguration effectively adjusts these windows online as long as we detect a significant decrease in the acceptance rate for a request.

Challenge #2: Selecting the best draft methods without priori knowledge (§4.2). Selecting the best draft method is critical to ensuring high speedup yet is quite challenging because the optimal draft method for each prompt varies and is unknown a priori. The diversity stems from the variation in acceptance rates for a given request. Figure 7 illustrates the speedup of different draft methods on different requests from a batch collected from the training trace. We can see that although many requests achieve the highest speedup with 0.5B drafting models, some require 1.5B models and others require statistical methods like n-gram. Directly executing

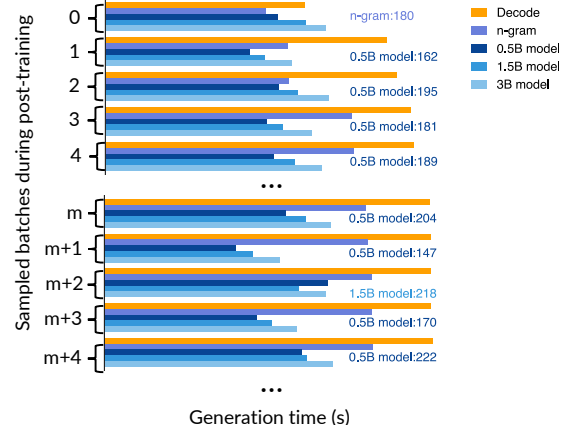


Figure 7: A characterization of the speedup of different draft methods on DAPO-32B-20K (see §5.1) training trace.

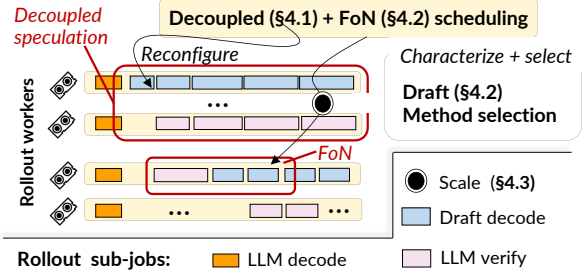


Figure 8: The system architecture of SPECACTOR.

multiple draft methods in parallel is infeasible because it requires significantly more GPUs—not only to host multiple draft models but also to verify their outputs.

Our solution: Fastest-of-N speculation. (§4.2) At the start of the rollout, we use the profiled acceptance rate to select the estimated best draft method, based on the observation that although each prompt’s acceptance rate varies significantly, for a large batch, the average acceptance rate is statistically stable. Thus, the selection based on the average is likely to be close to the optimal for the batch. The best draft is selected based on a ladder we constructed offline, which holistically considers major methods, including model-based [31] and n-gram-based [2, 16].

During the rollout, when more GPUs are freed due to finished requests, SPECACTOR dynamically utilizes freed GPUs to deploy more draft methods for tailed requests, where parallel drafting naturally approximates the best draft method better, because as long as the fastest draft method generates all the tokens, we can treat the requests as finished. As shown in Figure 6 (d), if worker 3 becomes idle, we add the second-best draft method (1.5B) to accelerate the unfinished requests. Note that in the illustration we only add one more verification instance since the drafter can be piggybacked on other workers as it is relatively lightweight. If the 1.5B drafting model finishes earlier, the request is completed, and the request is also removed from other workers (e.g., worker 0 and 1).

System architecture. Figure 8 shows the system architec-

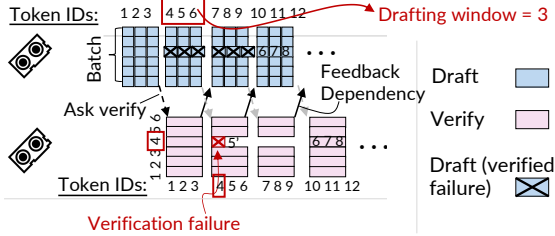


Figure 9: An illustration of how relaxed decoupled execution handles verification failure with a draft window of 3 tokens.

ture of SPECACTOR: a global scheduler searches an efficient decoupled speculation plan (§4.1) during the initial rollout phase. Each worker dynamically reconfigures the execution plan for low-acceptance-rate requests at runtime to improve efficiency. The global scheduler monitors the GPU usage across workers to deploy additional draft methods for long-tailed requests (§4.2). Our runtime (§4.3) efficiently supports scaling primitives required for Fastest-of-N speculation.

4 Detailed Design and Implementation

4.1 Efficient Decoupled Speculative Rollout

Methodology. We adopt a two-step scheduling method to realize an efficient decoupled speculation: (1) at the beginning of the rollout step, we determine the optimal placement—how many workers are assigned to drafting and verification, respectively—to minimize batch completion time. During rollout, we (2) dynamically monitor the acceptance rate of running requests to timely adjust their number of aggressively drafted tokens (with a draft window) to minimize the impact of verification failures.

We choose to adjust only the draft window per request but not the entire placement for the running batch during rollout for three reasons. First, the optimal placement relies on the modeling of system execution, but it becomes less accurate due to the continuously reduced batch sizes caused by finished requests. Second, the overhead of reconfiguring placement may outweigh the benefits. Finally, since the batch sizes shrink quickly thanks to our decoupled execution with optimal initial placement, we no longer need to maximize computational efficiency, and the fine-grained adjustment of the tail requests provided by (2) enables sufficient speedups.

Below, we first describe how we control the wasted tokens via *draft window*, and then proceed to the two policies.

Drafting window (w) and relaxed draft–verification dependency.

To control the waste due to mis-speculation, we set a window similar to previous works [40] such that: once the drafter sends w tokens to the verifier, it is only allowed to aggressively draft another w tokens. If the verifier has not finished verification, the drafter stops waiting for the feedback from the verifier. In this way, the drafter wastes at most $2w - 1$ tokens under speculation failures, as shown in Figure 9.

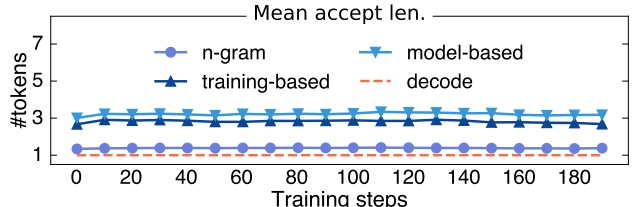


Figure 10: Mean acceptance length profiled in a 200-step DAPO-32B-20K trace, covering 327 K sequences. The training-based method uses *frozen* EAGLE released by TLT [23].

1. Decoupled speculation execution plan. At the beginning of each rollout step, given a draft method (described in §4.2), the trained model, and the available GPUs, our planner determines an appropriate draft window for the entire batch, and an efficient initial decoupled speculation plan by assigning the drafter and verifier to different GPUs. The plan only needs to be executed once during post-training because for each step, the initial batch size per worker remains the same, and the acceptance length—average output length per verification are stable for mainstream drafters, as shown in Figure 10. Our reported EAGLE acceptance length² is lower than that of TLT [23] because our rollout temperature is set to 1.0 and we use a large-batch-tuned configuration—a common production setup in post-training [13, 54, 4].

Finding the optimal execution plan requires solving a combination problem of the parallel configurations of different drafters and verifiers, as well as precisely modeling the performance of speculative decoding using the draft window. To ease problem formulation, we follow prior works that assume the developers have provided a set of possible GPU configurations for running a verifier (\mathbb{G}), i.e., how one copy of model parameter is partitioned on a set of GPUs. For drafter, we assume it only uses one GPU as it is lightweight.

Algorithm 1 describes our algorithm, which is essentially an enumeration-based search with decoupled-execution-aware pruning to accelerate the process. First, given a batch of requests to generate (i.e., B), we select a verification configuration (line 2), and estimate its performance under decoupled execution (TGS_{cur}) for various numbers of draft GPUs (line 3) and various draft window sizes (line 6). We continuously select execution plans and finally choose the one with the minimal estimated generation time (line 8–10).

To improve search time, we prune the enumeration space by (1) using the observation that drafters need fewer GPUs than verifiers (line 3) and (2) pruning arbitrarily large draft windows, because it only increases the computation waste upon mis-speculation (line 5).

Modeling TGS. A key aspect of the planning is to model the performance—token generation speed (TGS)—for decoupled execution. We use a bottom-up approach that first models the execution time of drafter and verifier, then move on the modeling of the expectation of TGS, considering the impact

²No prompt tuning was applied following TLT authors’ instructions.

of wasted tokens due to mis-speculation under a selected draft window.

Given a batch of request b , the number of drafter workers g_d , and a verifier with execution configuration g_v , the draft ($D_{g_d}(\cdot)$) and verification ($V_{g_v,w}(\cdot)$) time can be approximated as an affine function with respective to the batch size (b):

$$D_{g_d}(b) = b \cdot D'_{g_d} + \alpha_{g_d}$$

$$V_{g_v,w}(b) = b \cdot V'_{g_v,w} + \beta_{g_v,w}$$

where D'_{g_d} , $V'_{g_v,w}$, α_g and $\beta_{g_v,w}$ are hyperparameters that fitted through offline profiling, similar to prior works [82, 12].

Therefore, the total generation time of w tokens in our decoupled execution paradigm can be modeled as:

$$\text{IL}_{g_d,g_v,w}(b) = \max\{wD_{g_d}(b), V_{g_v,w}(b)\}$$

Besides the execution time, we also need to consider the slowdown due to mis-speculation. Given a draft window w and the probability of accepting one token p for a batch of requests, we follow prior works [26, 40] that first model the probability of accepting a tokens given n tokens within a draft window, then calculate the expected wasted tokens accordingly. The difference is that we further consider the additional wasted tokens due to aggressive speculation in decoupled execution. Specifically, within a draft window, the probability of accepting a tokens given an estimated accept probability (p) is:

$$P(a, w) = \begin{cases} p^a(1-p), & 0 \leq a \leq w-1, \\ p^a, & a = w, \end{cases}$$

s.t. $a \in \mathbb{N}, n \in \mathbb{Z}^+$

p is profiled using the setup from previous steps and we found it is quite stable for a relatively large batch of requests (see Figure 10).

The expectation of the total generated tokens for drafting a draft window w is:

$$\tau_w = \sum_{a=0}^{w-1} \underbrace{p^a(1-p)}_{\text{partial accept}} \frac{a+1}{2} + \underbrace{wp^w}_{\text{full accept}}$$

which is a summation of the expected generated tokens when the token is accepted at different positions.

Put it all together, the expectation of TGS is:

$$\text{TGS}_{g_d,g_v,w}(b) = \frac{\tau_w}{\text{IL}_{g_d,g_v,w}(b)}$$

2. Dynamic request-level reconfiguration. During decoupled execution, we dynamically monitor each request's acceptance rate to adjust its draft window accordingly. Algorithm 2 summarizes our reconfiguration algorithm, which is called periodically during the rollout.

Algorithm 1: Decoupled execution plan generation algorithm at the start of the rollout. $\text{TGS}_{g_d,g_v,w}(b)$, $V_{g_v,w}(b)$ and $D_{g_d}(b)$ are described in §4.1.

Input: Initial global batch size B , the number of GPUs in the cluster G , a set of execution configurations for verification \mathbb{G} .

Output: GPUs for drafting g_d^* , GPUs for verification g_v^* and draft window w^* .

```

1  $\text{TGS}^* \leftarrow 0, (g_d^*, g_v^*, w^*) \leftarrow (0, 0, 0)$ 
2 foreach GPU number  $g_v \in \mathbb{G}$  do
3   foreach GPU number  $g_d \leftarrow 1$  to  $g_v$  do
4      $b \leftarrow \lceil \frac{(g_d+g_v)B}{G} \rceil$ 
5      $w_{\max} = \max\{\lceil \frac{V'_{g_v,w}}{D'_{g_d}} \rceil, \lceil \frac{\beta_{g_v,w}}{\alpha_{g_d}} \rceil\}$ 
6     for  $w \leftarrow 1$  to  $w_{\max}$  do
7        $\text{TGS}_{\text{cur}} \leftarrow \text{TGS}_{g_d,g_v,w}(b)$ 
8       if  $\text{TGS}_{\text{cur}} > \text{TGS}^*$  then
9         update  $\text{TGS}^*$  and  $(g_d^*, g_v^*, w^*)$ 
10 return  $(g_d^*, g_v^*, w^*)$ 

```

Upon invocation, the algorithm first examines the set of requests with lower acceptance rates than the average (line 1), and reuses the performance model described above for decoupled execution and an extended modeling of coupled execution ($\text{TGS}_{C,w}(\cdot)$, omitted due to space limitation, since its modeling logic is similar to decoupled modeling) to enumerate the best configuration.

Three aspects need to be noted regarding online reconfiguration. First, we do not trigger reconfiguration too frequently because (1) the acceptance rate may change sharply over a short period, and (2) overly frequent reconfiguration may introduce performance instability. Currently, we reconfigure the system every 1000 decoding iterations. Second, we execute requests with different window sizes concurrently to maximize GPU utilization. To achieve efficient co-execution, we schedule kernels with different draft windows into a fused CUDA graph [1, 40]. Finally, switching between coupled and decoupled execution is straightforward, as we only need to pause the aggressive draft of the switched request.

4.2 Effective Fastest-of-N (FoN) Speculative Rollout

This section describes how we select draft methods for the rollout. The goal is to select the method with the highest speedup. The challenge lies in balancing the draft efficiency and the acceptance rate, given that the acceptance rate is unknown prior to execution for a given request.

To tackle this challenge, we leverage the fact that it is possible to estimate the speedup of different draft methods parameterized by the acceptance rate via offline profiling. With this information, selecting draft methods greedily using the average acceptance rate of a batch request is possible at

Algorithm 2: Request-level Reconfiguration for Reducing mis-speculation overheads during the rollout.

Input: pre-searched decoupled plan (g_d^*, g_v^*, w^*) , the set of requests with lower acceptance rate than average \mathbb{R} .

Output: Per-request draft plan $\{(w_r, m_r)\}_{r \in \mathbb{R}}$, w_r is request draft window, m_r is a flag specifying coupled (C) or decoupled (D) speculation.

```

1 foreach request  $r \in \mathbb{R}$  do
2    $p \leftarrow \text{ProfileProbability}(r)$ 
3    $w_c, \text{tgs}_c \leftarrow \arg \max_w \text{TGS}_{c,w}(p, b = 1)$ 
4    $w_d, \text{tgs}_d \leftarrow \arg \max_w \text{TGS}_{g_d^*, g_v^*, w}(p, b = 1)$ 
5    $w_r, m_r \leftarrow \text{SelectBetter}((w_c, \text{tgs}_c), (w_d, \text{tgs}_d))$ 
6 return  $\{(w_r, m_r) : r \in \mathbb{R}\}$ 

```

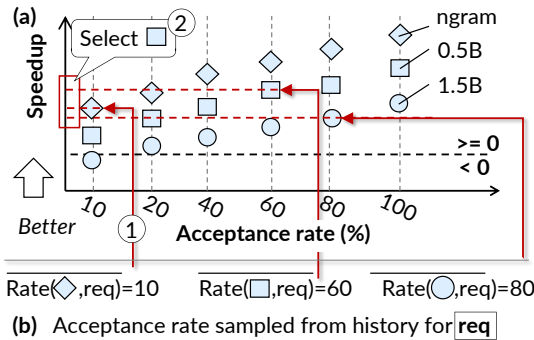


Figure 11: (a) Our draft ladder provides hints to the speedup of different draft methods and (b) our ranking (①) and selection (②) mechanism for choosing a draft method.

the beginning of the rollout, and we can further improve the selection based on the runtime-collected acceptance rate.

Draft ladder. A draft ladder provides information on the speedup of different draft methods given a fixed acceptance rate, as shown in Figure 11 (a). It can be efficiently constructed via offline profiling without using the trained model because (1) the execution of the drafter is irrelevant to the training model and (2) the speedup can be simulated by randomly accepting tokens according to a given acceptance rate. Thus, our offline profiler directly run the draft methods with simulated acceptance rate to build the ladder.

Our current ladder considers popular draft methods, including model-based [31, 43] and n-gram-based [2, 16, 25]. For model-based draft, we use a checkpoint from the same series as the large model, released jointly before the post-training pipeline. The practice is similar to previous inference works [31, 43], but we cannot use the thinking version draft models as they are typically distilled after the large thinking model is ready [13, 67]. We have also considered more draft methods, including training-based drafters such as the EAGLE family [35, 34, 36]. We do not include MTP [14] as it

Algorithm 3: Greedy Fastest-of-N assignments. b_{max} is the maximal verification batch size.

Input: the active requests set \mathbb{R} , the candidate draft methods set \mathbb{D} . W_d is the set of workers responsible for draft method d , and \mathbb{W} the whole set of free rollout workers.

Output: added drafters and the involved requests $\mathcal{M} = \{(r, d) : w\}_{r \in \mathbb{R}, d \in \mathbb{D}, w \in \mathbb{W}}$.

```

1  $\mathcal{R} \leftarrow \text{sort } \mathbb{R} \text{ by GetAcceptRate}(r) \text{ ascending}$ 
2  $\mathcal{D} \leftarrow \text{sort } \mathbb{D} \text{ by GetLadderRank}(d) \text{ ascending}$ 
3 foreach request  $r \in \mathbb{R}$  do
4   foreach draft method  $d \in \mathbb{D}$  do
5     if  $\mathcal{M}(r, d)$  is None then
6        $w \leftarrow \text{GetMinLoadWorker}(\mathbb{W}_d, b_{max})$ 
7       if  $w$  is not None then
8          $\mathcal{M}(r, d) \leftarrow w$ 
9          $\text{load}(w) += 1$ 
10 return  $\mathcal{M}$ 

```

is not integrated by our evaluated models. Nevertheless, we should emphasize that our design is orthogonal to the draft methods, and integrating more draft methods is likely to make SPECACTOR faster if they can further improve speculation speedup.

Draft method selection at the beginning of the rollout.

Initially, we select *one* draft method for the entire batch based on the historically profiled acceptance rate. The profiling only needs to be done once, as the profiled results are stable across different steps (see Figure 10). We cannot select multiple methods because each drafter requires similar amount of verification, and we have insufficient GPU computational power during the initial phase.

Figure 11 (b) illustrates the selection process: For three exemplified draft methods—n-gram, drafting with a 0.5B and 1.5B model, we first query the profiled acceptance rate of these methods, and use these rates as the estimated acceptance rate of the batch. Based on the rate, we can estimate the speedup of each draft method (①) and then select the fastest one among them (②).

Greedy Fastest-of-N assignments. To cope with the sub-optimal initial selection for tailed requests, we greedily deploy more draft methods as soon as GPUs of both drafter and verifier become available upon batch completion. Algorithm 3 shows our algorithm for assigning more drafters (and their corresponding verifier) when there are available workers. The routine is iteratively called once there are free workers.

The algorithm assigns drafters to requests in an order sorted by the reverse of their acceptance rate (lines 1) as these requests have little speedup with speculative decoding. For each request, we add a drafter with the highest speedup according to the draft ladder described before if it has not been assigned

yet (line 2 and 5). We greedily assign as many drafters as possible to the request until there are no available workers or pending requests (lines 3–9). If the assignments for a request are completed, we proceed to the next request.

Here we adopt a draft-first design that assigns as many draft methods to one request as possible before moving on to the next one. The rationale is that the request with the lowest acceptance rate is likely to suffer from suboptimal drafting, so the draft-first strategy can naturally select the optimal draft method for it (given a sufficient number of free workers). In case of an insufficient number of free workers, we prioritize the draft method with a higher rank in our draft ladder.

Discussion for evolvable draft methods. Our ladder assumes that the draft models are frozen during the post-training, because we found that the acceptance rate of draft methods remains stable across steps (even with long gap), see Figure 10. We suspect this is because even as the trained model becomes smarter, many trivial tokens can still be drafted as long as the trained model corrects the incorrect tokens timely. Note that recent draft training optimizations [23] is orthogonal to our design as they can also be applied to our small models. Further, integrating such evolving would require intrusive modifications to both the rollout and training engines. Therefore, we don’t include them in our implementation.

4.3 Efficient System Runtime for SPECACTOR

SPECACTOR only optimizes the rollout phase and makes no intrusive modifications to the training engine, in contrast to [80, 18]. The runtime extension is also lightweight: supporting decoupled execution only requires message passing between the drafter and the verifier, and we further incorporate two primitives to support Fastest-of-N speculation:

Model scale. The primitive deploys a serving instance—either a drafter or a verifier—to a specific worker. This is similar to model autoscaling in existing serving engines [17, 66, 62, 74, 75] and we adopted all their designs, including pre-pinning serving engines on workers [66], pre-materializing CUDA graphs with GPU execution context pools [74, 62] and transfer model weights via fast networking between GPUs [75]. To further eliminate the overhead of loading large trained model weights to GPUs especially in case of deploying a new verifier, we observed that verifiers are deployed only to freed drafters and the drafter GPUs have low GPU memory usage due to the small size of draft models. Thus, we further pin the trained models to drafters to enable a zero-cost verifier deployment.

KVCache scale. Besides the model, when scaling a new drafter’s corresponding verifier, the new verifier requires a copy of the KVCache—the intermediate results of the LLM computation—to accelerate computation. A challenge is that during the later stage of rollout, the KVCache may become large since its size is proportional to the model size and the number of generated tokens. To this end, we can leverage the

classic KVCache recovery method, which transfers the tail KVCache through the network and recomputes it from the beginning [29] to accelerate the KVCache scaling.

5 Evaluation

5.1 Experimental setup

We implemented SPECACTOR on veRL—the state-of-the-art post-training framework that has integrated known inference optimizations including CUDA graph [1], prefix caching [54] and FlashAttention kernels [53].

Testbed. We evaluated SPECACTOR on a production training cluster with up to 512 GPUs. These GPUs are organized into nodes where each node contains eight Hopper (80 GB) GPUs interconnected with 400 GB/s NVLink, and inter-node GPUs have up to 400 Gbps RDMA connections.

Evaluated traces: model, algorithm and rollout temperature. Similar to prior works [71, 55, 79], we evaluated Qwen series models (e.g., Qwen2.5-32B) as they are one of the most popular open-sourced LLMs [71, 72, 78] and are commonly used by algorithm designers. We evaluated on 3 representative 200-step training traces based on production setups with different (popular) post-training algorithms:

- **GRPO-32B-20K.** This trace trains Qwen2.5-32B [61] with the GRPO [54] algorithm, a representative value-model-free post-training method that trains high-quality models like DeepSeek series [76, 13]. The trace samples a total batch of 8,192 prompts at each step³, where for each batch, the model generates responses with a budget of 20 K tokens. The trace runs on 256 GPUs with a tensor parallelism (TP) degree of 4 for each rollout worker, so the initial per-worker batch size is 128.
- **DAPO-32B-20K.** This trace also trains Qwen2.5-32B using DAPO [71]—a trending algorithm in AI academy and industry [19, 68]—with a per-step batch size of 16,384 and a response budget of 20 K tokens. The trace runs on 256 GPUs with a 4-degree TP for each rollout worker, so the per-worker batch size is 256. DAPO requires a larger per-step batch size because its training method filters out low-quality responses generated during the rollout.
- **PPO-32B-20K.** PPO is another widely used RL algorithm [52, 72]. The trained model is Qwen2.5-32B, and the PPO trace is different in (1) it utilizes another 32B critic model to generate value and trains the critic together with the actor model; (2) meanwhile, it samples only one response per prompt. The per-step batch size is 4,096 and the maximum response length is 20 K tokens. We run the trace on the same cluster setup like the above two traces.

For all experiments, we set the sampling temperature of LLM generation to 1.0—a common setup in post-training [13, 54, 4]—which, however, has a negative impact on speculative

³Including the group sampling factor.

decoding [65, 58, 11]. LLM post-training requires such settings to explore more diverse responses and avoid entropy collapse [20, 71, 72]; otherwise, the trained model suffers from premature convergence, which limits its potential for further performance gains.

Due to GPU time constraints, our experiments focus on dense 32 B models, but we have also conducted experiments on a large Qwen3-235B MoE model [67] in §5.3 to demonstrate the effectiveness of SPECACTOR.

Evaluating metrics. We focus on reporting the end-to-end training time and the rollout time—since training time is the most critical metric for algorithm developers and rollout dominates the time in §2.1. To ensure representative evaluation, we uniformly sample at least 10% of all training steps, using the trained checkpoints at the sampled steps for generation, and report their training and rollout time.

Baselines. We compared SPECACTOR with the following baselines and carefully tuned their implementations and performance. All systems rollout with vLLM v0.10.0 engine [1]. Specifically, the decoding latency of Qwen2.5-32B model is lower to 13 ms when per-worker batch size is 1 on our platform. For all baselines, we report the optimal configuration for training, i.e., an FSDP degree of 32 and 8-way sequence parallelism [27].

- **veRL** [56] is an open-sourced post-training system used by SEED and SPECACTOR is based on it. Besides the inference optimizations mentioned in the beginning of the section, it further incorporates techniques like efficient parameter to quickly update parameters for the rollout.
- **RLHFuse** [80] is the state-of-the-art post-training system that overlaps the prepare and rollout phases to reduce bubbles caused by long-tailed generation. Since it is not open-sourced, we carefully re-implemented its design and achieve a similar speedup on short-context tasks.
- **veRL (2 ×)** provisions 2 × of GPUs used by the original trace for veRL, which serves as the optimal performance of using more GPUs to accelerate RL like RLBoost [6].
- **veRL + (vanilla) model-spec.** To illustrate the effectiveness of our proposed techniques, we also compare veRL by incorporating model-based speculative decoding in inference systems [31, 43]. We run coupled speculation described in §3. The draft method is selected based on the first phase of our Fastest-of-N speculation. For 32B training, we found 0.5B is a sweet point to accelerate.
- **veRL + (vanilla) n-gram.** N-gram is a popular speculative decoding method used by other works [21, 48] to accelerate rollout. We have integrated a baseline of it using vLLM’s n-gram (v0.10.0), with enhancement of recent techniques like SAM [25] to match their implementation as much as possible (since their code is not open-sourced).

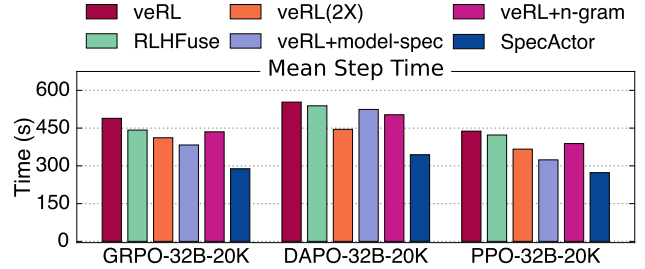


Figure 12: The mean training step time of SPECACTOR running different training traces with different approaches.

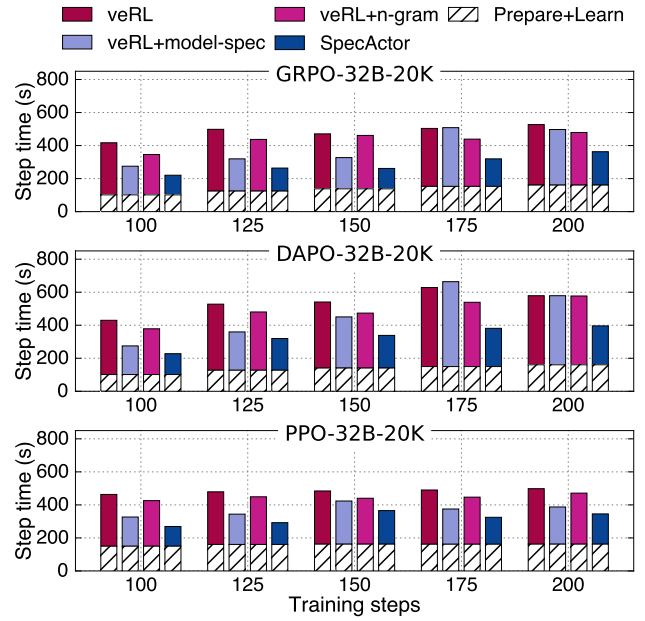


Figure 13: A breakdown of post-training process of different approaches on different training traces.

Draft methods used by SPECACTOR. Unless otherwise specified, we select the available drafters for Qwen2.5-32B before the post-training pipeline: Qwen2.5-0.5B [61], Qwen2.5-1.5B—as well as an n-gram drafter [1, 25]. Other drafting methods, such as EAGLE [35, 34, 36], require additional training support, which is not supported by all our evaluated models.

5.2 End-to-end post-training performance

Figure 12 presents the end-to-end training step time of different approaches on the traces. We measure all 1/10 of the sampled training steps and report the mean step time of different approaches. Note that each step uses the exact same model checkpoint and prompt batch in the trace to faithfully reproduce the real-world workloads. SPECACTOR achieves 1.5–1.7 × faster end-to-end training compared to baselines like veRL and RLHFuse. For vanilla speculative decoding baselines, SPECACTOR achieves 1.2–1.5 × shorter training time in different traces. Even compared with veRL

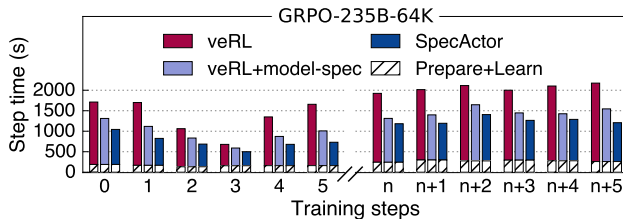


Figure 14: A breakdown of post-training steps of Qwen3-235B.

($2 \times$) that uses twice the GPUs, SPECACTOR still achieves $1.3\text{--}1.4 \times$ training speedup. The key contributor is the acceleration of rollout via our efficient mechanisms: for the rollout phase, SPECACTOR achieves $2.0\text{--}2.4 \times$ faster mean generation speed than veRL.

Notably, SPECACTOR achieves up to $1.4\text{--}2.0 \times$ shorter average rollout time even compared with methods that also incorporate speculative decoding acceleration, i.e., model-spec and n-gram. This is because: First, both of them suffer from inefficiency due to large per-worker batch size in the initial phase. Second, both of them, especially n-gram, have low acceptance rates for the straggler requests, because the n-gram method performs poorly in high temperature sampling with few history prompts commonly found in training traces. Specifically, the skipped iteration of the last finished requests of n-gram is $16.9\text{--}43.6\%$ across the traces, while SPECACTOR achieves $40.9\text{--}73.5\%$ thanks to our Fastest-of-N speculation.

5.3 Performance on large MoE models

Figure 14 presents the performance of SPECACTOR when training a Qwen3-235B MoE model [67] on 256 GPUs with GRPO algorithm. Due to limited GPU time and the availability of checkpoints, we only evaluated a few steps: 0–5 at the start of the post-training (using the Qwen3-235B-Instruct-2507) and $n, \dots, n+5$ from the end of the training (using the Qwen3-235B-Thinking-2507). The difference is that the later steps tend to generate longer responses. The per-step batch size is 256—a slightly smaller batch size due to limited GPU memory, and each rollout worker uses expert parallelism (EP) of 8 for high decode efficiency.

We expand the draft ladder with small models produced before post-training pipeline [67]: Qwen3-4B-2507-Instruct (released together with 235B), Qwen3-0.6B and Qwen3-1.7B.

SPECACTOR improves the training time by $1.4\text{--}2.3 \times$, with $1.5\text{--}2.6 \times$ rollout acceleration compared to veRL. It also outperforms vanilla mode-spec by $1.1\text{--}1.5 \times$, thanks to our decoupled and Fastest-of-N speculation. Notice that even with a relatively small per-step batch size, verification overhead is still high in MoE models as it is exacerbated by expert communication [26]. We also found that Qwen3-4B-2507-Instruct performs significantly better in speculation than the other two, we suspect its training pipeline is closely coupled with 235B and thus has better alignment with it.

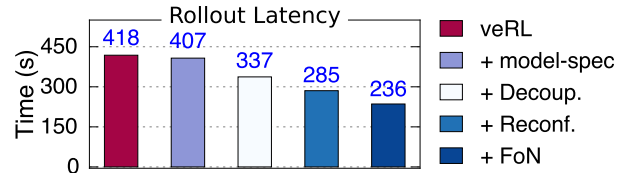


Figure 15: Ablation study of using the DAPO-32B-20K trace. The other trace shows similar results.

5.4 Performance across different steps

As the trained model evolves across different training steps, the effectiveness of speculative decoding varies. Thus, we further present the detailed latency breakdown of different training steps in Figure 13. For ease of presentation, we selectively present part of the training steps between 100–200 training steps to examine speculative decoding’s effect in real-world post-training. The gap is sufficiently large as confirmed by internal accuracy tests, so the “smartness” of the trained models in different sampling steps varies.

First we can see that SPECACTOR still achieves the shortest rollout time in all steps. Specifically, at 175th and 200th steps, veRL + model-spec and n-gram fail to provide acceleration because as models becomes smarter, they tend to produce longer responses [13] for more prompts, leading to more rollout steps under a relatively large per-worker batch size. In contrast, SPECACTOR consistently reduces rollout time by $1.8\text{--}2.7 \times$, and is faster than vanilla speculative decoding baselines by $1.4\text{--}2.6 \times$, $1.2\text{--}2.2 \times$, $1.2\text{--}2.6 \times$ in different training traces. Thanks to the quick generation, more workers finish at early time, leaving SPECACTOR sufficient room for FoN scheduling.

5.5 Ablation study

Figure 15 conducts an ablation study to examine the effectiveness of different proposed techniques described in §4. We reported only one step here due to space limitation, and other steps in different traces show similar results.

First, we can see that vanilla speculative decoding reduces only 2.6 % rollout end-to-end latency, which is small due to the inefficiency of large-batch verification and suboptimal draft method for the tailed requests.

Thanks to our decoupled speculative decoding, we accelerate rollout by $1.3 \times$. Based on decoupled speculative decoding, our dynamic reconfiguration further shortens the rollout time by $1.2 \times$ thanks to a better initial execution configuration and dynamic reconfiguration of workers with low acceptance rates to reduce wasted tokens. Finally, our Fastest-of-N speculative decoding further accelerates end-to-end rollout by $1.2 \times$, thanks to its ability to leverage multiple draft methods to improve acceptance rates for straggler requests.

5.6 An in-depth look at SPECACTOR in action

We conclude our evaluation of SPECACTOR by presenting an in-depth analysis of the work done by different workers

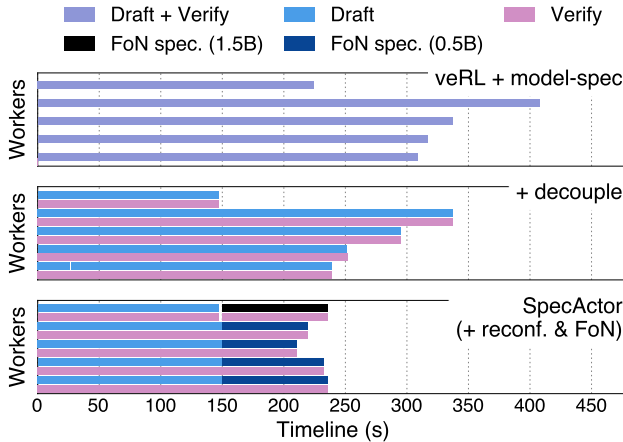


Figure 16: An in-depth analysis of the execution of different approaches on the 200th step of DAPO-32B-20K trace. We sample workers that contains the tailed requests for ease of presentation.

during the rollout with our techniques in Figure 16. To ease presentation, we only sampled 5 workers, with a deliberate focus on the worker that finish early and the slowest four workers.

First, from the first row of Figure 16 we can see that vanilla speculative decoding still suffers from long-tailed workers because during the initial phase all workers execute slower and at the end the initially selected draft method cannot accelerate the slowest requests. With decoupled speculative decoding (the second row), we improve speculative decoding performance by 1.1–1.5 × but still suffer from long-tailed requests due to suboptimal draft method. With Fastest-of-N speculative decoding activated, the freed workers are assigned different draft methods (we use different color blocks to indicate different draft methods) at 151s in Figure 16. This subsequently accelerates the slowest requests by 1.5 ×.

6 Related work

Rollout acceleration with algorithmic modifications. Several works propose algorithmic changes to accelerate rollout, e.g., skipping the tail generations [60, 10, 21]. Such modifications essentially make the training a variant of off-policy (vs. on-policy of our targeted setup), which has unstable convergence in theory [3, 50, 59] and we observe that they are not always adopted in production [48, 13].

Rollout acceleration for resource-restrict setups. Recent works like Seer [48] and RollPacker [18] address long-tail generation in resource-constraint setups, i.e., each worker has limited GPU capacity to hold the assigned batch. As a result, the batch must be further divided into sub-batches where each sub-batch is executed sequentially, and their optimizations lie in reordering or repacking sub-patches to reduce GPU wastes between sub-batch executions. In contrast, SPECACTOR accelerates long-tail generations where the batch can fit in the GPU memory of each worker, a common production setup

(see Figure 5 (a)). In general, executing one large batch is faster than sequentially executing the divided sub-batch (if with sufficient resources) because the generation time grows sub-linearly with the batch size (see Figure 5 (b)), not to mention the possible switching overhead between sub-batches with packing techniques [18].

Concurrent works on accelerating rollout via speculative decoding. A few concurrent works share a similar high-level idea of using speculative decoding to accelerate rollout [23, 48]. SPECACTOR further addresses the low efficiency issue in batch configurations that are unfriendly to speculative decoding, and the unknown best drafter selection issue across requests.

The closest work to ours is TLT [23], which selects training-based drafter (EAGLE [35, 34, 36]) for speculative rollout. It does not consider the large batch efficiency issue and its performance can be further improved with our decoupled speculation. Moreover, our draft ladder with Fastest-of-N speculation further provides two advantages over its chosen EAGLE: (1) EAGLE is more challenging to deploy than the model- and n-gram-based methods in our ladder because it requires extra training to match the target model [34, 36], which is not always available for the trained model or requires extra tuning; and (2) we found it has a lower acceptance length than the drafters we considered using the models provided by TLT without prompt tuning for EAGLE [49] (see Figure 10). Finally, TLT adopts approximate sampling to improve the acceptance rate at the cost of training accuracy [11]. In contrast, SPECACTOR uses exact matching to ensure the correctness of the rollout responses.

Speculative decoding in inference. The optimization goal of using speculative decoding in rollout is fundamentally different from that in inference systems [31, 43, 38, 77, 39, 40]. Specifically, rollout prioritizes overall batch execution efficiency, where individual request latencies are less critical, while inference systems must ensure low latencies for all requests. This introduces new challenges, which we address with decoupled and Fastest-of-N speculation.

7 Conclusion

This paper shows that RL rollout can be efficient without compromising the algorithmic equivalence of the original training with fast speculative decoding. SPECACTOR makes speculative rollout efficient with two novel techniques: (1) a *Decoupled speculation* method that improves the speculation efficiency for common training setups, and (2) a *Fastest-of-N speculation* method that dynamically adapts the draft method during the rollout process. SPECACTOR improves the training efficiency by 1.4–2.3 × compared to the state-of-the-art baselines, and is 1.1–2.6 × faster than vanilla speculative rollout.

References

[1] Easy, fast, and cheap llm serving for everyone. <https://github.com/v11m-project/v11m>, 2024.

[2] APOORV SAXENA, A. T. S. Prompt lookup decoding. <https://github.com/apoorvumang/prompt-lookup-decoding>, 2025.

[3] ARNAL, C., NAROZNIAK, G., CABANNES, V., TANG, Y., KEMPE, J., AND MUNOS, R. Asymmetric REINFORCE for off-policy reinforcement learning: Balancing positive and negative rewards. *CoRR abs/2506.20520* (2025).

[4] BAI, Y., BAO, Y., CHEN, G., AND ET. AL. Kimi K2: open agentic intelligence. *CoRR abs/2507.20534* (2025).

[5] BAI, Y., JONES, A., NDOUSSE, K., AND ET.AL. Training a helpful and harmless assistant with reinforcement learning from human feedback. *CoRR abs/2204.05862* (2022).

[6] BATANERO, E. A., PASCUAL, Á. F., AND JIMÉNEZ, Á. B. RL-boost: Boosting supervised models using deep reinforcement learning. *Neurocomputing 618* (2025), 128815.

[7] BEHRENS, J., CAO, A., SKEGGS, C., BELAY, A., KAASHOEK, M. F., AND ZELDOVICH, N. Efficiently mitigating transient execution attacks using the unmapped speculation contract. In *14th USENIX Symposium on Operating Systems Design and Implementation, OSDI 2020, Virtual Event, November 4-6, 2020* (2020), USENIX Association, pp. 1139–1154.

[8] CHANG, F. W., AND GIBSON, G. A. Automatic I/O hint generation through speculative execution. In *Proceedings of the Third USENIX Symposium on Operating Systems Design and Implementation (OSDI), New Orleans, Louisiana, USA, February 22-25, 1999* (1999), M. I. Seltzer and P. J. Leach, Eds., USENIX Association, pp. 1–14.

[9] CHEN, C., BORGEAUD, S., IRVING, G., LESPIAU, J., SIFRE, L., AND JUMPER, J. Accelerating large language model decoding with speculative sampling. *CoRR abs/2302.01318* (2023).

[10] CHEN, J., FAN, T., LIU, X., AND ET. AL. Seed1.5-thinking: Advancing superb reasoning models with reinforcement learning. *CoRR abs/2504.13914* (2025).

[11] CHEN, Q., LIU, Z., SUN, P., LI, S., WANG, G., LIU, Z., WEN, Y., FENG, S., AND ZHANG, T. Respec: Towards optimizing speculative decoding in reinforcement learning systems. *CoRR abs/2510.26475* (2025).

[12] CHENG, R., LAI, Y., WEI, X., CHEN, R., AND CHEN, H. Kunserve: Parameter-centric memory management for efficient memory overloading handling in llm serving. *CoRR abs/2412.18169* (2024).

[13] DAYA GUO, DEJIAN YANG, H. Z. E. A. Deepseek-r1 incentivizes reasoning in llms through reinforcement learning. *Nature 645* (2025), 633–638.

[14] DEEPSEEK-AI. Deepseek-v3 technical report. *CoRR abs/2412.19437* (2024).

[15] DEEPSEEK-AI, GUO, D., YANG, D., ZHANG, H., AND ET. AL. Deepseek-r1: Incentivizing reasoning capability in llms via reinforcement learning. *CoRR abs/2501.12948* (2025).

[16] FU, Y., BAILIS, P., STOICA, I., AND ZHANG, H. Break the sequential dependency of LLM inference using lookahead decoding. In *Forty-first International Conference on Machine Learning, ICML 2024, Vienna, Austria, July 21-27, 2024* (2024), OpenReview.net.

[17] FU, Y., XUE, L., HUANG, Y., BRABETE, A., USTIUGOV, D., PATEL, Y., AND MAI, L. Serverlessllm: Low-latency serverless inference for large language models. In *18th USENIX Symposium on Operating Systems Design and Implementation, OSDI 2024, Santa Clara, CA, USA, July 10-12, 2024* (2024), A. Gavrilovska and D. B. Terry, Eds., USENIX Association, pp. 135–153.

[18] GAO, W., ZHAO, Y., AN, D., WU, T., CAO, L., XIONG, S., HUANG, J., WANG, W., YANG, S., SU, W., WANG, J., QU, L., ZHENG, B., AND WANG, W. Rollpacker: Mitigating long-tail rollouts for fast, synchronous RL post-training. *CoRR abs/2509.21009* (2025).

[19] GOLUBEV, A., TROFIMOVA, M., POLEZHAEV, S., BADERT-DINOV, I., NEKRASHEVICH, M., SHEVTSOV, A., KARASIK, S., ABRAMOV, S., ANDRIUSHCHENKO, A., FISIN, F., SKVORTSOV, S., AND YANGEL, B. Training long-context, multi-turn software engineering agents with reinforcement learning. *CoRR abs/2508.03501* (2025).

[20] HAO, Y., DONG, L., WU, X., HUANG, S., CHI, Z., AND WEI, F. On-policy RL with optimal reward baseline. *CoRR abs/2505.23585* (2025).

[21] HE, J., LI, T., FENG, E., DU, D., LIU, Q., LIU, T., XIA, Y., AND CHEN, H. History rhymes: Accelerating LLM reinforcement learning with rhymarl. *CoRR abs/2508.18588* (2025).

[22] HOEFFDING, W. Probability inequalities for sums of bounded random variables. *Journal of the American statistical association 58*, 301 (1963), 13–30.

[23] HU, Q., YANG, S., GUO, J., YAO, X., LIN, Y., GU, Y., CAI, H., GAN, C., KLIMOVIC, A., AND HAN, S. Taming the long-tail: Efficient reasoning rl training with adaptive drafter. *CoRR abs/2511.16665* (2025).

[24] HU, T., LIAKOPOULOS, D., WEI, X., MARCULESCU, R., AND YADWADKAR, N. J. Simulating rumor spreading in social networks using LLM agents. *CoRR abs/2502.01450* (2025).

[25] HU, Y., WANG, K., ZHANG, X., ZHANG, F., LI, C., CHEN, H., AND ZHANG, J. SAM decoding: Speculative decoding via suffix automaton. In *Proceedings of the 63rd Annual Meeting of the Association for Computational Linguistics (Volume 1: Long Papers), ACL 2025, Vienna, Austria, July 27 - August 1, 2025* (2025), W. Che, J. Nabende, E. Shutova, and M. T. Pilehvar, Eds., Association for Computational Linguistics, pp. 12187–12204.

[26] HUANG, Z., ZHU, L., ZHAN, Z., HU, T., MAO, W., YU, X., LIU, Y., AND ZHANG, T. Moesd: Unveil speculative decoding’s potential for accelerating sparse moe. *CoRR abs/2505.19645* (2025).

[27] JACOBS, S. A., TANAKA, M., ZHANG, C., ZHANG, M., SONG, S. L., RAJBANDARI, S., AND HE, Y. Deepspeed ulysses: System optimizations for enabling training of extreme long sequence transformer models. *CoRR abs/2309.14509* (2023).

[28] JIMENEZ, C. E., YANG, J., WETTIG, A., YAO, S., PEI, K., PRESS, O., AND NARASIMHAN, K. R. Swe-bench: Can language models resolve real-world github issues? In *The Twelfth International Conference on Learning Representations, ICLR 2024, Vienna, Austria, May 7-11, 2024* (2024), OpenReview.net.

[29] JIN, S., LIU, X., ZHANG, Q., AND MAO, Z. M. Compute or load KV cache? why not both? *CoRR abs/2410.03065* (2024).

[30] KESKAR, N. S., MUDIGERE, D., NOCEDAL, J., SMELYANSKIY, M., AND TANG, P. T. P. On large-batch training for deep learning: Generalization gap and sharp minima. In *5th International Conference on Learning Representations, ICLR 2017, Toulon, France, April 24-26, 2017, Conference Track Proceedings* (2017), OpenReview.net.

[31] LEVIATHAN, Y., KALMAN, M., AND MATIAS, Y. Fast inference from transformers via speculative decoding. In *International Conference on Machine Learning, ICML 2023, 23-29 July 2023, Honolulu, Hawaii, USA* (2023), A. Krause, E. Brunskill, K. Cho, B. Engelhardt, S. Sabato, and J. Scarlett, Eds., vol. 202 of *Proceedings of Machine Learning Research*, PMLR, pp. 19274–19286.

[32] LEVIATHAN, Y., KALMAN, M., AND MATIAS, Y. Fast inference from transformers via speculative decoding. In *International Conference on Machine Learning, ICML 2023, 23-29 July 2023, Honolulu, Hawaii, USA* (2023), A. Krause, E. Brunskill, K. Cho, B. Engelhardt, S. Sabato, and J. Scarlett, Eds., vol. 202 of *Proceedings of Machine Learning Research*, PMLR, pp. 19274–19286.

[33] LI, J., SHEN, J., SU, Y., AND LYU, M. R. Llm-assisted mutation for whitebox API testing. *CoRR abs/2504.05738* (2025).

[34] LI, Y., WEI, F., ZHANG, C., AND ZHANG, H. EAGLE-2: faster inference of language models with dynamic draft trees. In *Proceedings of the 2024 Conference on Empirical Methods in Natural Language Processing, EMNLP 2024, Miami, FL, USA, November 12-16, 2024* (2024), Y. Al-Onaizan, M. Bansal, and Y. Chen, Eds., Association for Computational Linguistics, pp. 7421–7432.

[35] LI, Y., WEI, F., ZHANG, C., AND ZHANG, H. EAGLE: speculative sampling requires rethinking feature uncertainty. In *Forty-first International Conference on Machine Learning, ICML 2024, Vienna, Austria, July 21-27, 2024* (2024), OpenReview.net.

[36] LI, Y., WEI, F., ZHANG, C., AND ZHANG, H. EAGLE-3: scaling up inference acceleration of large language models via training-time test. *CoRR abs/2503.01840* (2025).

[37] LIU, B., WANG, A., MIN, Z., YAO, L., ZHANG, H., LIU, Y., ZENG, A., AND SU, J. Spec-rl: Accelerating on-policy reinforcement learning via speculative rollouts, 2025.

[38] LIU, T., LI, Y., LV, Q., LIU, K., ZHU, J., HU, W., AND SUN, X. PEARL: parallel speculative decoding with adaptive draft length. In *The Thirteenth International Conference on Learning Representations, ICLR 2025, Singapore, April 24-28, 2025* (2025), OpenReview.net.

[39] LIU, X., HU, L., BAILIS, P., CHEUNG, A., DENG, Z., STOICA, I., AND ZHANG, H. Online speculative decoding. In *Forty-first International Conference on Machine Learning, ICML 2024, Vienna, Austria, July 21-27, 2024* (2024), OpenReview.net.

[40] LIU, X., PARK, J., HU, L., KWON, W., LI, Z., ZHANG, C., DU, K., MO, X., YOU, K., CHEUNG, A., DENG, Z., STOICA, I., AND ZHANG, H. Turbospec: Closed-loop speculation control system for optimizing llm serving goodput. *CoRR abs/2405.14088* (2025).

[41] LIU, X., YU, H., ZHANG, H., AND ET. AL. Agentbench: Evaluating llms as agents. In *The Twelfth International Conference on Learning Representations, ICLR 2024, Vienna, Austria, May 7-11, 2024* (2024), OpenReview.net.

[42] MEI, Z., FU, W., LI, K., WANG, G., ZHANG, H., AND WU, Y. Realhf: Optimized RLHF training for large language models through parameter reallocation. *CoRR abs/2406.14088* (2024).

[43] MIAO, X., OLIARO, G., ZHANG, Z., CHENG, X., WANG, Z., ZHANG, Z., WONG, R. Y. Y., ZHU, A., YANG, L., SHI, X., SHI, C., CHEN, Z., ARFEEN, D., ABHYANKAR, R., AND JIA, Z. Specinfer: Accelerating large language model serving with tree-based speculative inference and verification. In *Proceedings of the 29th ACM International Conference on Architectural Support for Programming Languages and Operating Systems, Volume 3, ASPLOS 2024, La Jolla, CA, USA, 27 April 2024- 1 May 2024* (2024), R. Gupta, N. B. Abu-Ghazaleh, M. Musuvathi, and D. Tsafir, Eds., ACM, pp. 932–949.

[44] MIAO, X., OLIARO, G., ZHANG, Z., CHENG, X., WANG, Z., ZHANG, Z., WONG, R. Y. Y., ZHU, A., YANG, L., SHI, X., SHI, C., CHEN, Z., ARFEEN, D., ABHYANKAR, R., AND JIA, Z. Specinfer: Accelerating large language model serving with tree-based speculative inference and verification. In *Proceedings of the 29th ACM International Conference on Architectural Support for Programming Languages and Operating Systems, Volume 3, ASPLOS 2024, La Jolla, CA, USA, 27 April 2024- 1 May 2024* (2024), R. Gupta, N. B. Abu-Ghazaleh, M. Musuvathi, and D. Tsafir, Eds., ACM, pp. 932–949.

[45] NAKANO, R., HILTON, J., BALAJI, S., WU, J., OUYANG, L., KIM, C., HESSE, C., JAIN, S., KOSARAJU, V., SAUNDERS, W., JIANG, X., COBBE, K., ELOUNDOU, T., KRUEGER, G., BUTTON, K., KNIGHT, M., CHESS, B., AND SCHULMAN, J. Webgpt: Browser-assisted question-answering with human feedback. *CoRR abs/2112.09332* (2021).

[46] OPENAI. GPT-4 technical report. *CoRR abs/2303.08774* (2023).

[47] PARK, J., CHO, S., AND HAN, D. Specedge: Scalable edge-assisted serving framework for interactive llms. *CoRR abs/2505.17052* (2025).

[48] QIN, R., HE, W., HUANG, W., ZHANG, Y., ZHAO, Y., PANG, B., XU, X., SHAN, Y., WU, Y., AND ZHANG, M. Seer: Online context learning for fast synchronous llm reinforcement learning. *CoRR abs/2511.14617* (2025).

[49] QINGHAO HU, S. Y. Tl github (fastrl). <https://github.com/mit-han-lab/fastrl>, 2025.

[50] ROUX, N. L., BELLEMARE, M. G., LEBENSOLD, J., BERGERON, A., GREAVES, J., FRÉCHETTE, A., PELLETIER, C., THIBODEAU-LAUFER, E., TÓTH, S., AND WORK, S. Tapered off-policy REINFORCE: stable and efficient reinforcement learning for llms. *CoRR abs/2503.14286* (2025).

[51] ROZIÈRE, B., GEHRING, J., GLOECKLE, F., SOOTLA, S., GAT, I., TAN, X. E., ADI, Y., LIU, J., REMEZ, T., RAPIN, J., KOZHEVNIKOV, A., EVTIMOV, I., BITTON, J., BHATT, M., CANTON-FERRER, C., GRATTAFIORI, A., XIONG, W., DÉFOSSEZ, A., COPET, J., AZHAR, F., TOUVRON, H., MARTIN, L., USUNIER, N., SCIALOM, T., AND SYNNAEVE, G. Code llama: Open foundation models for code. *CoRR abs/2308.12950* (2023).

[52] SCHULMAN, J., WOLSKI, F., DHARIWAL, P., RADFORD, A., AND KLIMOV, O. Proximal policy optimization algorithms. *CoRR abs/1707.06347* (2017).

[53] SHAH, J., BIKSHANDI, G., ZHANG, Y., THAKKAR, V., RAMANI, P., AND DAO, T. Flashattention-3: Fast and accurate attention with asynchrony and low-precision. In *Advances in Neural Information Processing Systems 38: Annual Conference on Neural Information Processing Systems 2024, NeurIPS 2024, Vancouver, BC, Canada, December 10 - 15, 2024* (2024), A. Globersons, L. Mackey, D. Belgrave, A. Fan, U. Paquet, J. M. Tomczak, and C. Zhang, Eds.

[54] SHAO, Z., WANG, P., ZHU, Q., XU, R., SONG, J., ZHANG, M., LI, Y. K., WU, Y., AND GUO, D. Deepseekmath: Pushing the limits of mathematical reasoning in open language models. *CoRR abs/2402.03300* (2024).

[55] SHENG, G., ZHANG, C., YE, Z., WU, X., ZHANG, W., ZHANG, R., PENG, Y., LIN, H., AND WU, C. Hybridflow: A flexible and efficient RLHF framework. In *Proceedings of the Twentieth European Conference on Computer Systems, EuroSys 2025, Rotterdam, The Netherlands, 30 March 2025 - 3 April 2025* (2025), ACM, pp. 1279–1297.

[56] SHENG, G., ZHANG, C., YE, Z., WU, X., ZHANG, W., ZHANG, R., PENG, Y., LIN, H., AND WU, C. Hybridflow: A flexible and efficient RLHF framework. In *Proceedings of the Twentieth European Conference on Computer Systems, EuroSys 2025, Rotterdam, The Netherlands, 30 March 2025 - 3 April 2025* (2025), ACM, pp. 1279–1297.

[57] STERN, M., SHAZER, N., AND USZKOREIT, J. Blockwise parallel decoding for deep autoregressive models. In *Advances in Neural Information Processing Systems 31: Annual Conference on Neural Information Processing Systems 2018, NeurIPS 2018, December 3-8, 2018, Montréal, Canada* (2018), S. Bengio, H. M. Wallach, H. Larochelle, K. Grauman, N. Cesa-Bianchi, and R. Garnett, Eds., pp. 10107–10116.

[58] SUN, S., LI, Y., LI, X., LIAN, Y., LIN, W., ZHEN, H., YANG, Z., CHEN, C., YU, X., YUAN, M., AND MA, C. Scaling up, speeding up: A benchmark of speculative decoding for efficient LLM test-time scaling. *CoRR abs/2509.04474* (2025).

[59] TANG, Y., GUO, Z. D., ZHENG, Z., CALANDRIELLO, D., CAO, Y., TARASSOV, E., MUNOS, R., PIRES, B. Á., VALKO, M., CHENG, Y., AND DABNEY, W. Understanding the performance gap between online and offline alignment algorithms. *CoRR abs/2405.08448* (2024).

[60] TEAM, K., DU, A., GAO, B., AND ET.AL. Kimi k1.5: Scaling reinforcement learning with llms. *CoRR abs/2501.12599* (2025).

[61] TEAM, Q. Qwen2.5: A party of foundation models, September 2024.

[62] WEI, X., HUANG, Z., SUN, T., HAO, Y., CHEN, R., HAN, M., GU, J., AND CHEN, H. Phoenixos: Concurrent os-level GPU checkpoint and restore with validated speculation. In *Proceedings of the ACM SIGOPS 31st Symposium on Operating Systems Principles, SOSP 2025, Lotte Hotel World, Seoul, Republic of Korea, October 13-16, 2025* (2025), Y. Won, Y. Kwon, D. Yuan, and R. Isaacs, Eds., ACM, pp. 996–1013.

[63] WILLIAMS, D., CRAUN, M., LE, M. V., STEPHEN, J. J., AHMED, S., AND JAMJOOM, H. Towards safe agentic AI performance engineering. In *Proceedings of the 4th Workshop on Practical Adoption Challenges of ML for Systems, PACMI 2025, Seoul, Republic of Korea, October 13-16, 2025* (2025), ACM, pp. 63–68.

[64] WU, B., LIU, S., ZHONG, Y., SUN, P., LIU, X., AND JIN, X. Loongserve: Efficiently serving long-context large language models with elastic sequence parallelism. In *Proceedings of the ACM SIGOPS 30th Symposium on Operating Systems Principles, SOSP 2024, Austin, TX, USA, November 4-6, 2024* (2024), E. Witchel, C. J. Rossbach, A. C. Arpaci-Dusseau, and K. Keeton, Eds., ACM, pp. 640–654.

[65] XIA, H., YANG, Z., DONG, Q., WANG, P., LI, Y., GE, T., LIU, T., LI, W., AND SUI, Z. Unlocking efficiency in large language model inference: A comprehensive survey of speculative decoding. In *Findings of the Association for Computational Linguistics, ACL 2024, Bangkok, Thailand and virtual meeting, August 11-16, 2024* (2024), L. Ku, A. Martins, and V. Srikumar, Eds., Association for Computational Linguistics, pp. 7655–7671.

[66] XIANG, Y., LI, X., QIAN, K., YANG, Y., ZHU, D., YU, W., ZHAI, E., LIU, X., JIN, X., AND ZHOU, J. Aegaeon: Effective GPU pooling for concurrent LLM serving on the market. In *Proceedings of the ACM SIGOPS 31st Symposium on Operating Systems Principles, SOSP 2025, Lotte Hotel World, Seoul, Republic of Korea, October 13-16, 2025* (2025), Y. Won, Y. Kwon, D. Yuan, and R. Isaacs, Eds., ACM, pp. 1030–1045.

[67] YANG, A., LI, A., YANG, B., AND ET. AL. Qwen3 technical report. *CoRR abs/2505.09388* (2025).

[68] YAO, J., CHENG, R., WU, X., WU, J., AND TAN, K. C. Diversity-aware policy optimization for large language model reasoning. *CoRR abs/2505.23433* (2025).

[69] YAO, Z., GHOLAMI, A., LEI, Q., KEUTZER, K., AND MAHONEY, M. W. Hessian-based analysis of large batch training and robustness to adversaries. In *Advances in Neural Information Processing Systems 31: Annual Conference on Neural Information Processing Systems 2018, NeurIPS 2018, December 3-8, 2018, Montréal, Canada* (2018), S. Bengio, H. M. Wallach, H. Larochelle, K. Grauman, N. Cesa-Bianchi, and R. Garnett, Eds., pp. 4954–4964.

[70] YE, N., AHUJA, A., LIARGKOVAS, G., LU, Y., KAFFES, K., AND PENG, T. Speculative actions: A lossless framework for faster agentic systems. *CoRR abs/2510.04371* (2025).

[71] YU, Q., ZHANG, Z., ZHU, R., YUAN, Y., ZUO, X., YUE, Y., FAN, T., LIU, G., LIU, L., LIU, X., LIN, H., LIN, Z., MA, B., SHENG, G., TONG, Y., ZHANG, C., ZHANG, M., ZHANG, W., ZHU, H., ZHU, J., CHEN, J., CHEN, J., WANG, C., YU, H., DAI, W., SONG, Y., WEI, X., ZHOU, H., LIU, J., MA, W., ZHANG, Y., YAN, L., QIAO, M., WU, Y., AND WANG, M. DAPO: an open-source LLM reinforcement learning system at scale. *CoRR abs/2503.14476* (2025).

[72] YUE, Y., YUAN, Y., YU, Q., ZUO, X., ZHU, R., XU, W., CHEN, J., WANG, C., FAN, T., DU, Z., WEI, X., YU, X., LIU, G., LIU, J., LIU, L., LIN, H., LIN, Z., MA, B., ZHANG, C., ZHANG, M., ZHANG, W., ZHU, H., ZHANG, R., LIU, X., WANG, M., WU, Y., AND YAN, L. VAPO: efficient and reliable reinforcement learning for advanced reasoning tasks. *CoRR abs/2504.05118* (2025).

[73] ZAN, D., HUANG, Z., LIU, W., CHEN, H., ZHANG, L., XIN, S., CHEN, L., LIU, Q., ZHONG, X., LI, A., LIU, S., XIAO, Y., CHEN, L., ZHANG, Y., SU, J., LIU, T., LONG, R., SHEN, K., AND XIANG, L. Multi-swe-bench: A multilingual benchmark for issue resolving. *CoRR abs/2504.02605* (2025).

[74] ZENG, S., XIE, M., GAO, S., CHEN, Y., AND LU, Y. Medusa: Accelerating serverless LLM inference with materialization. In *Proceedings of the 30th ACM International Conference on Architectural Support for Programming Languages and Operating Systems, Volume 1, ASPLOS 2025, Rotterdam, The Netherlands, 30 March 2025 - 3 April 2025* (2025), L. Eeckhout, G. Smaragdakis, K. Liang, A. Sampson, M. A. Kim, and C. J. Rossbach, Eds., ACM, pp. 653–668.

[75] ZHANG, D., WANG, H., LIU, Y., WEI, X., SHAN, Y., CHEN, R., AND CHEN, H. Blitzscale: Fast and live large model autoscaling with O(1) host caching. In *19th USENIX Symposium on Operating Systems Design and Implementation, OSDI 2025, Boston, MA, USA, July 7-9, 2025* (2025), L. Zhou and Y. Zhou, Eds., USENIX Association, pp. 275–293.

[76] ZHANG, G., GENG, H., YU, X., YIN, Z., ZHANG, Z., TAN, Z., ZHOU, H., LI, Z., XUE, X., LI, Y., ZHOU, Y., CHEN, Y., ZHANG, C., FAN, Y., WANG, Z., HUANG, S., LIAO, Y., WANG, H., YANG, M., JI, H., LITTMAN, M., WANG, J., YAN, S., TORR, P., AND BAI, L. The landscape of agentic reinforcement learning for llms: A survey. *CoRR abs/2509.02547* (2025).

[77] ZHANG, Z., JIANG, Z., JIANG, C., YU, M., ZHENG, S., LIN, H., HOFFMANN, H., AND LIU, X. Swiftspec: Ultra-low latency LLM decoding by scaling asynchronous speculative decoding. *CoRR abs/2506.11309* (2025).

[78] ZHENG, C., LIU, S., LI, M., CHEN, X.-H., YU, B., GAO, C., DANG, K., LIU, Y., MEN, R., YANG, A., ZHOU, J., AND LIN, J. Group sequence policy optimization, 2025.

[79] ZHONG, Y., ZHANG, Z., SONG, X., HU, H., JIN, C., WU, B., CHEN, N., CHEN, Y., ZHOU, Y., WAN, C., ZHOU, H., JIANG, Y., ZHU, Y., AND JIANG, D. Streamrl: Scalable, heterogeneous, and elastic RL for llms with disaggregated stream generation. *CoRR abs/2504.15930* (2025).

[80] ZHONG, Y., ZHANG, Z., WU, B., LIU, S., CHEN, Y., WAN, C., HU, H., XIA, L., MING, R., ZHU, Y., AND JIN, X. Optimizing RLHF training for large language models with stage fusion. In *22nd USENIX Symposium on Networked Systems Design and Implementation, NSDI 2025, Philadelphia, PA, USA, April 28-30, 2025* (2025), T. A. Benson and R. N. Mysore, Eds., USENIX Association, pp. 489–503.

[81] ZHONG, Y., ZHANG, Z., WU, B., LIU, S., CHEN, Y., WAN, C., HU, H., XIA, L., MING, R., ZHU, Y., AND JIN, X. Optimizing RLHF training for large language models with stage fusion. In *22nd USENIX Symposium on Networked Systems Design and Implementation, NSDI 2025, Philadelphia, PA, USA, April 28-30, 2025* (2025), T. A. Benson and R. N. Mysore, Eds., USENIX Association, pp. 489–503.

[82] ZHU, K., GAO, Y., ZHAO, Y., ZHAO, L., ZUO, G., GU, Y., XIE, D., YE, Z., KAMAHORI, K., LIN, C., WANG, Z., WANG, S., KRISHNAMURTHY, A., AND KASIKCI, B. Nanoflow: Towards optimal large language model serving throughput. In *19th USENIX Symposium on Operating Systems Design and Implementation, OSDI 2025, Boston, MA, USA, July 7-9, 2025* (2025), L. Zhou and Y. Zhou, Eds., USENIX Association, pp. 749–765.